ELSEVIER

Thin Solid Films 322 (1998) 263–273

thin solid films

A comparison of the electrochemical behaviour of W–M–N (M = Ni, Ti, Al) thin film coatings on high speed steel

Christopher M.A. Brett [a,*], Albano Cavaleiro [b]

[a] *Departamento de Química, Universidade de Coimbra, 3049 Coimbra, Portugal*
[b] *Departamento de Engenharia Mecânica, Universidade de Coimbra, 3030 Coimbra, Portugal*

Received 4 August 1997; accepted 30 October 1997

Abstract

The electrochemical behaviour of W–M–N (M = Ni, Ti, Al) thin-film hard coatings on high speed steel has been studied. Films of 4 μm thickness of W–Ni, W–Ti and W–Ti–Al with and without nitrogen were produced by DC diode sputtering. Electrochemical measurements were carried out in aqueous potassium chloride solution. Open circuit potential measurements, Tafel plots and electrochemical impedance all show the importance of the influence of nitrogen on the coating behaviour, and some differences between coating types due to the combination of metallic elements are evident. Corrosion is localised at specific points in the coating, which appear in the first hour after immersion. They exhibit the same general features in all cases, involving corrosion beneath the coating followed by film rupture. Electrochemical observations are supported by scanning electron microscopy observations, X-ray diffraction and microindentation measurements before and after corrosion has taken place. A model describing the corrosion process is developed and discussed.

Keywords: Hard coatings; Thin films; Tungsten-based coatings; Corrosion; High speed steel

1. Introduction

In recent years much effort has been devoted to research into thin-film sputtered coatings. Such coatings are frequently prepared with a view to increasing the hardness of the substrate and/or its corrosion resistance. As almost all materials can be deposited by the sputtering technique, a suitable choice of the target allows the formation of thin films with a wide variation of chemical composition. Moreover, the introduction in the sputtering chamber of gases at low pressures, such as nitrogen, oxygen or methane, permits their incorporation in the growing coating and, under some conditions, the obtaining of a large range of compounds (nitrides, oxides, carbides). Sputtering is also the most appropriate technique for the production of materials with metastable structures. After a careful selection of the deposition conditions it is possible to obtain materials with approximately the same chemical composition but with structures far from thermodynamic equilibrium, such as amorphous or high temperature phases.

Much effort regarding wear and corrosion resistance has been directed towards nitride coatings prepared by physical vapour deposition, such as TiN and CrN [1–6]. Work has also been directed towards alloy coatings. These include corrosion resistance investigations on a variety of amorphous surface alloys [7]. Our work has been particularly aimed towards characterisation of tungsten-containing coatings of the type W–C–(Co) [8–12] for wear resistance applications, whose corrosion resistance has also been studied [13], and more recently of the type W–M–(N), where M = Ti or Ni, regarding their oxidation behaviour and corrosion resistance [14–17].

In this article a comparison is made between the corrosion resistance of films of the type W–Ni–N, W–Ti–N and W–Ti–Al–N. The interest in the inclusion of aluminium in the films is the possible increase in corrosion resistance; aluminium–titanium alloys have already been the object of some investigation [18] as has the interaction between Al films and W–Ti films [19].

2. Experimental

Substrates were heat-treated discs, diameter 12 mm and thickness 3 mm, of M2 high speed steel (W 6.4; Mo 5.0;

* Corresponding author.

0040-6090/98/$19.00

Table 1
Characteristics of the sputtered W–M–N films on M2 steel (at %)

Film	W	Ni	Ti	Al	N
W–Ni	97.3	2.7	–	–	–
W–Ni–N	66.5	12.1	–	–	21.4
W–Ti	72.2	–	27.8	–	–
W–Ti–N	24.8	–	21.2	–	54.0
W–Ti–Al	54.9	–	39.7	5.4	–
W–Ti–Al–N	23.2	–	21.7	4.3	50.8

Cr 4.2; V 1.9; C 0.86; Si < 0.4; Mn < 0.4 wt.%) as described elsewhere [16]. After polishing to a mirror finish on a polishing table with diamond paste they were sputter-coated on one face in a Hartec DC diode sputtering apparatus. After cleaning the surface by heating and argon ion etching, deposition was done from the appropriate target at a power density of 11 W cm^{-2} and a negative substrate bias of 70 V. Target compositions were: W + 10 wt.% Ni, W + 20 wt.% Ti and W + 25 wt.% Ti + 5 wt.% Al. The total gas pressure employed during deposition was 0.3 Pa; the gas was a mixture of nitrogen and argon, the partial pressure of nitrogen being varied. Each sputtering deposition led to ten equal samples with uniform coating thickness. The compositions of the six types of coating employed in this comparative study are shown in Table 1.

Coated samples were transformed into electrodes by attaching a copper wire to the rear face with silver epoxy and protecting the whole assembly, except for the coated face, with epoxy resin and varnish. The electrochemical cell also contained a platinum foil counter electrode and a saturated calomel electrode as reference. All electrochemical experiments to be described were carried out using a solution of 0.1 M potassium chloride prepared from analytical grade reagent and ultrapure water (Millipore Milli-Q, resistivity > 18 MΩ cm). Solutions were not deaerated.

Corrosion potential measurements were made with a Schlumberger S17151 Computing Multimeter and voltammetric experiments with a PC-controlled EG&G PAR273 A potentiostat using PAR Model 352 software. Impedance measurements were carried out using a Solartron 1250 Frequency Response Analyser coupled to a Solartron 1286 Electrochemical Interface using a 5 mV rms perturbation in the frequency range 65 kHz to 10 MHz and controlled by ZPlot software; simulations were performed with ZSim CNLS software.

Scanning electron microscopy was done with a Jeol T330 Scanning Electron Microscope equipped with a Tracor Northern Microanalysis Accessory. X-ray diffractometry analysis (XRD) was used for phase identification (Philips, PW3040/00 X-PERTH). The hardness and Young's Modulus of coated samples were measured by the depth sensing indentation technique using a Fischerscope H100 with a nominal test load of 200 mN. The indentation hysteresis curves were analysed following the procedure described in a previous paper [20] which takes into account the imperfect shapes of the Vickers indenter and of the indentation itself.

3. Results and discussion

The purpose of this paper is the elaboration of models for corrosion of these types of sputtered coating in chloride media, and to what extent the mechanism and the rate

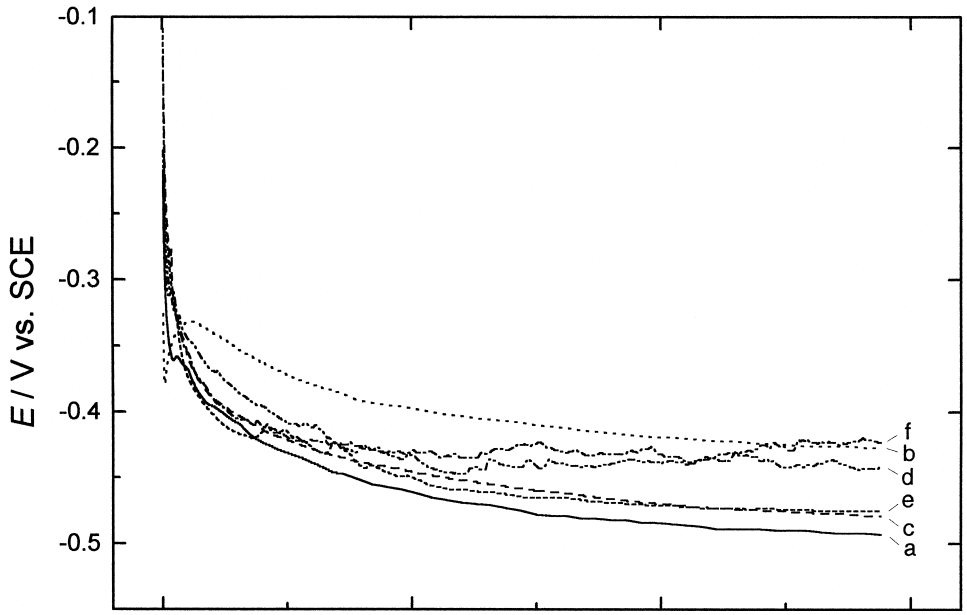

Fig. 1. Variation of corrosion potential with time for the six types of coating: (a) W–Ni; (b) W–Ni–N; (c) W–Ti; (d) W–Ti–N; (e) W–Ti–Al; (f) W–Ti–Al–N.

depend on film composition. To this end, two principal points of interest in this comparative study are the effects of different metallic alloying elements on the electrochemical behaviour of the coatings and the influence of the introduction of nitrogen. The high percentage of nitrogen introduced in films containing titanium (see Table 1) was not possible in W–Ni films owing to the considerably lesser affinity between Ni and nitrogen than Ti and nitrogen during reactive sputtering. Electrochemical and morphological observations will be discussed taking into account the film structure and a model for pitting corrosion will be put forward.

3.1. Open circuit potential

Corrosion potential values determined by open circuit potential measurements are shown in Fig. 1 and at two points in time in Table 2. There is a negative trend with increasing time, and eventually after periods superior to 10 h the values become those of the steel substrate [21]. Visual observation shows that corrosion is localised, as do the observed oscillations superimposed on the general variation with time, which can be attributed to pit birth and death phenomena. After covering the points of corrosion with epoxy glue, following 1 h immersion in chloride solution, the corrosion rate became lower, as demonstrated by a lower slope in the profile of corrosion potential vs. time, and periodic oscillations disappeared.

3.2. Voltammetric measurements

Measurements were made as soon as possible after immersion of the sample in the chloride solution (when film integrity is, in principle, assured) and changes with time were followed. Thus, the first linear polarisation resistance measurements (Table 3) were obtained after only a few minutes immersion. This was also done with Tafel plots, see examples in Fig. 2. Analysis of the Tafel plots by the ParCalc routine included with M352 software, and which optimises fitting of the experimental curve, are presented in Table 4. Comparison of E_{cor} values from Tafel plots leads to the conclusion that the introduction of nitrogen in the films is beneficial.

Corrosion currents have lowest values for W–Ni and W–Ni–N films, with the exception of W–Ti–Al films after 1 h and after 4 h. Interestingly, for W–Ti and W–Ti–Al films the introduction of nitrogen makes the corrosion potential more positive, but the corrosion current is also increased. This could be due to the formation of oxide at some points on the coating surface and will be further discussed in Section 3.3.

Table 2
Values of E_{cor} (vs. SCE) from open circuit potential measurements

Film	E_{cor} /V	
	$t = 2$ min	$t = 4$ h
W–Ni	−0.23	−0.49
W–Ni–N	−0.31	−0.43
W–Ti	−0.175	−0.475
W–Ti–N	−0.22	−0.44
W–Ti–Al	−0.125	−0.475
W–Ti–Al–N	−0.28	−0.42

Table 3
Results from linear polarization resistance measurements, R_p. Potential scanned from $E_{cor} - 10$ mV to $E_{cor} + 10$ mV at a scan rate of 0.1 mV s^{-1}

Film	R_p /kΩ cm^2	
	$t = 5$ min	$t = 1$ h
W–Ni	9.9	6.8
W–Ni–N	20.2	8.0
W–Ti	4.4	2.3
W–Ti–N	3.1	3.8
W–Ti–Al	5.8	9.7
W–Ti–Al–N	5.7	4.4

3.3. Electrochemical impedance

Electrochemical impedance experiments were performed at applied potentials corresponding to the corrosion potential. In all cases the general shape in the complex plane plot was that of a depressed semicircle. Fitting of the experimental data was possible by using the equivalent circuit shown in Fig. 3. This consists of an *RC* parallel element representing the substrate–film–solution interfacial region, where pitting corrosion occurs, in parallel with a series combination of bulk film resistance R_1 and distributed element, *DE*, representing constant phase angle characteristics due to film heterogeneity. Fig. 4 shows a typical example. Best fitting of the electrochemical impedance measurements gave the values shown in Table 5 and leads to the very clear conclusion that nitrogen increases film resistance. With time there is a tendency for the R_{ct} values to decrease.

3.4. Morphological observations

Scanning electron microscopy shows the same sort of pitting phenomena for all types of sample. Pits appear randomly over the sample surface but at a low density of between 10–20 pits cm^{-2}. After pit formation during the first hour, the number does not increase, but there is rather an increase in size of the existing pits. There is also some increase in surface roughness compared to the uncorroded samples.

The types of morphology corresponding to the pitting corrosion encountered are exemplified in Fig. 5 and are found on all types of coating examined. A pit usually shows a central area in which substrate corrosion is occurring—mainly of iron—surrounded by uncorroded film and debris of iron oxide hydrate at some distance from the

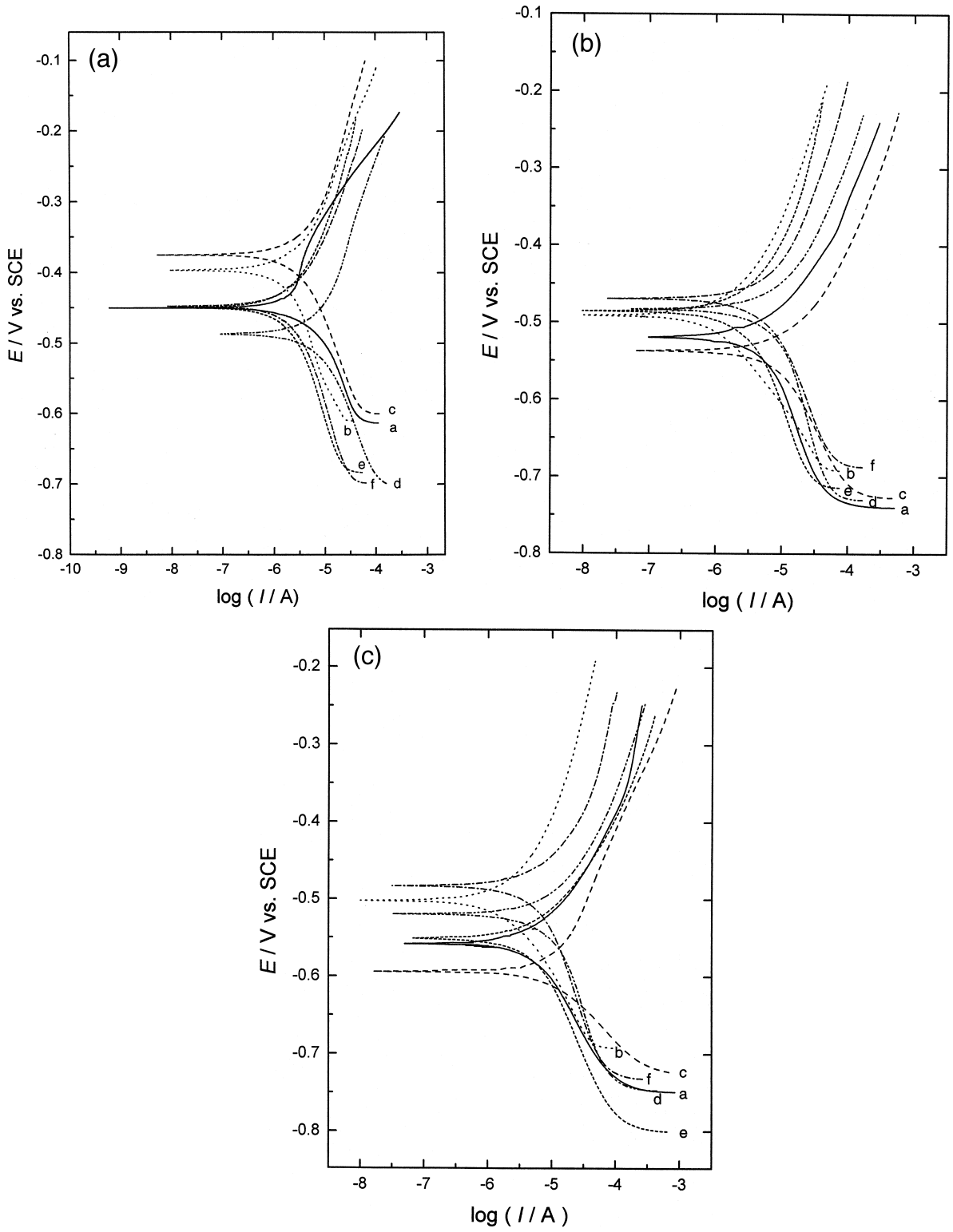

Fig. 2. Tafel plots for samples immersed for (a) 10 min (b) 1 h (c) 4 h. Scan rate 2 mV s^{-1} in positive direction. Sample identification as in Fig. 1.

central pit. This is demonstrated in Fig. 5a. Fig. 5b is an amplification of the right-hand pit in Fig. 5a which shows the collapse of a circular zone around the exposed substrate, suggesting that corrosion has occurred under this part of the film.

The crucial question is how the pits begin to grow. Evidence for this may be in the type of 'growth' at isolated points on the surface which have the same chemical composition as the sputtered film (Fig. 5c)—these occasionally have a visible fissure as shown previously [16].

Table 4
Data obtained from Tafel plots

Film	I_{cor} / μA cm^{-2}			$-E_{cor}$ /V		
	10 min	1 h	4 h	10 min	1 h	4 h
W–Ni	1.8	9.9	8.7	0.45	0.52	0.55
W–Ni–N	2.7	1.9	3.6	0.40	0.50	0.50
W–Ti	6.3	18.9	11.6	0.37	0.53	0.60
W–Ti–N	12.5	16.5	19.0	0.48	0.48	0.52
W–Ti–Al	3.8	6.2	7.0	0.45	0.48	0.55
W–Ti–Al–N	4.1	13.8	13.4	0.44	0.47	0.48

Indeed, some of the pits show remnants of this type of bubble at the edge as shown in Fig. 5d. The implication is that in these cases the bubble becomes unstable and either implodes (Fig. 5a) or explodes (Fig. 5d), the film then falling away from the sample. In both cases a circular feature is formed with accumulation of iron oxide debris at some distance from the exposed substrate, which sometimes forms before the bubble bursts (Fig. 5c).

3.5. Film structure

Three different types of structure were identified for the various coatings by X-ray diffraction (XRD). The b.c.c. α-W phase is found for films which have no nitrogen; the main difference between their X-ray spectra and that of pure tungsten is a shift in the position of diffraction peaks indicating that Ti, Ni and Al are in solid solution in the W lattice.

Films containing nitrogen show an NaCl-type f.c.c. phase corresponding to W_2N/TiN with the exception of the W–Ni–N coating which shows an amorphous structure. In the first case, owing to the close interplanar distances of W_2N and TiN, it is thought that a mixture of W and Ti atoms exists in the lattice positions of the f.c.c. phase [14,15]. For W–Ni–N, the amorphous structure was expected as obtained previously for similar W–C–Ni sputtered films [22]. It was demonstrated that, for Ni content higher than a threshold value ($\sim$ 10 at%), W–C–Ni films have an amorphous structure. Since there is sufficient nitrogen content and the %Ni is about 12%, then, if the role of nitrogen is similar to that of carbon, there exist conditions to form amorphous films.

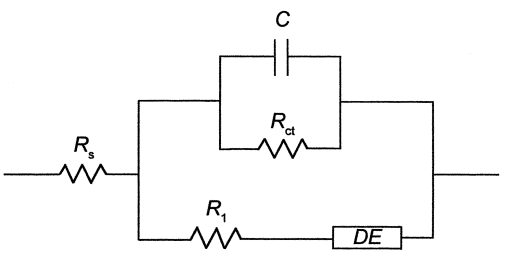

Fig. 3. Equivalent circuit used for modelling electrochemical impedance results. See text for explanation of symbols— R_s is the cell and bulk sample resistance ($\sim$ 30 Ω cm^2).

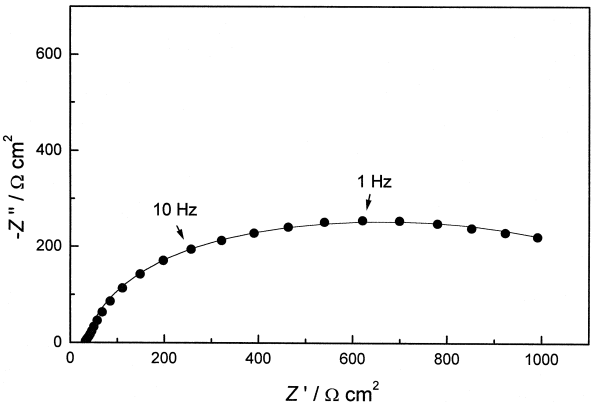

Fig. 4. Complex plane impedance plot from W–Ti sample after 1 h immersion: (●) experimental points, (————) simulation. Fitted values from equivalent circuit (Fig. 3) are $C = 18$ μF cm^{-2}, $R_{ct} = 1.34$ kΩ cm^{-2}, $R_s = 34$ Ω cm^2, $R_1 = 20$ Ω cm^2, constant phase angle = 0.19 π.

After corrosion very small changes in the X-ray diffraction spectra were observed on the corroded samples. Only very small new additional peaks were detected. Fig. 6 shows, as example, the X-ray spectra of two samples before and after corrosion. These small peaks can be indexed as iron oxide hydrate [23]. No signs of W, Ti or Al compounds were detected. These results are in good agreement with EDXS analysis carried out on the corrosion products, in which only the presence of iron was demonstrated.

3.6. A model for film corrosion

The electrochemical data gives evidence that corrosion in these films is extremely localised and only occurs in specific areas, of dimensions approximately between 5 and 30 μm diameter. Besides this, both X-ray diffraction results and ultramicroindentation analysis confirm that sample degradation takes place only at particular points and that the main corrosion products are from the substrate. Structural analysis shows only iron-containing corrosion products indicating that, if the degradation is extended to the entire sample surface, only a very thin protective layer can be formed, not detectable by X-ray

Table 5
Values of charge transfer resistance, R_{ct}, determined from impedance plots

Film	R_{ct} /kΩ cm^2	
	$t = 10$ min	$t = 1$ h
W–Ni	2.6	2.5
W–Ni–N	5.6	2.8
W–Ti	1.5	0.5
W–Ti–N	2.5	2.0
W–Ti–Al	3.5	1.5
W–Ti–Al–N	12.0	10.0

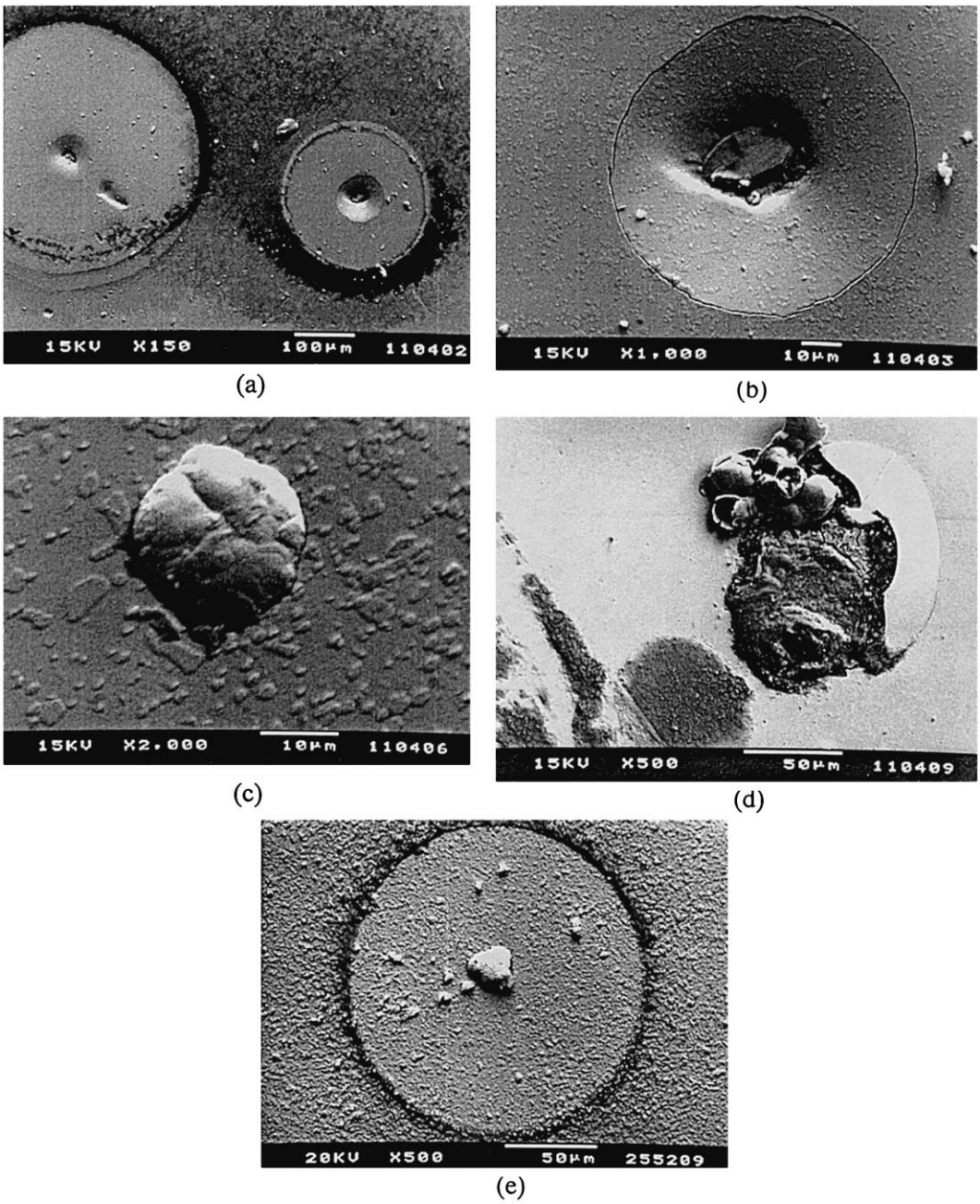

Fig. 5. Scanning electron micrographs showing pitting corrosion of films: (a), (b) W–Ti–Al–N; (c), (d) W–Ti–Al; (e) W–Ni.

diffraction. In another study, [24] it was shown that the hardness and the Young's Modulus of the coatings, determined by ultramicroindentation techniques, are similar before and after corrosion, indicating that there was no significant material degradation in those zones (see Fig. 7 as example of ultramicroindentation curves).

Once pits have formed at such points, no further pits appear (see glue protection experiments). Corrosion pits must form where there are film defects. However, examination of the surface of freshly-sputtered films shows no microscopic flaws so that these must be associated with sub-microscopic porosity. In the early period after immersion, the total number of pits found should be related to this sub-microscopic porosity induced by the process of film growth. It is well known that, varying the deposition conditions, it is possible to obtain a large variety of cross-section morphologies for sputtered coatings, ranging from columnar to very dense 'featureless' morphologies [11]. The presence of nitrogen in W–Ti, W–Ti–Al and W–Ni films gives rise to more compact morphologies, as already discussed by Dirks et al. [25] and as can be observed in Fig. 8 for W–Ti–(N) films. Thus, a large

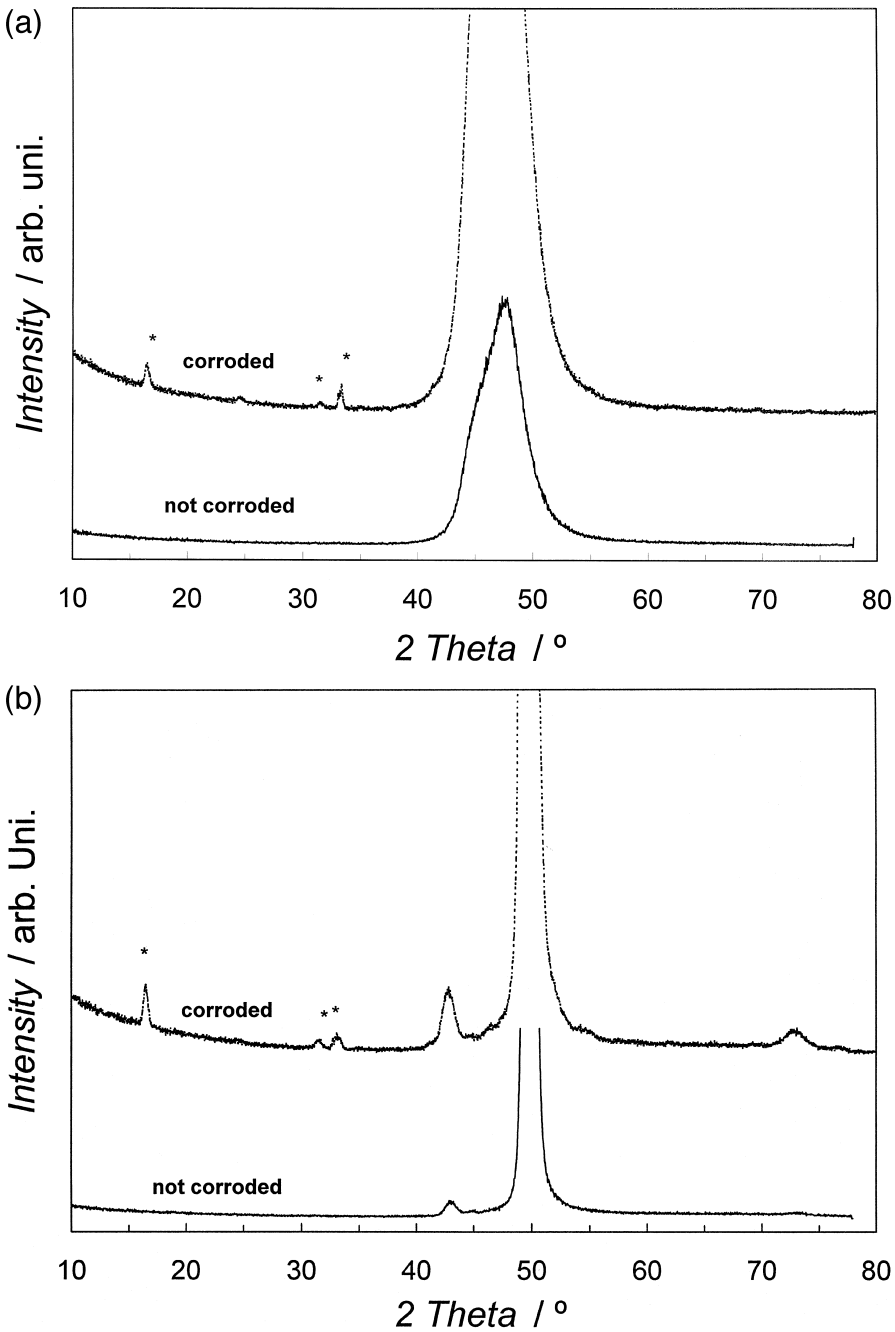

Fig. 6. X-ray diffraction spectra of W–Ti (a) and W–Ti–N (b) sputtered films before and after corrosion (*- diffraction peaks of iron oxide hydrate).

number of pits should be formed in films not containing N which is a possible first explanation for their worse corrosion resistance.

However, the influence of N on coating morphology is not the only factor that can explain the different corrosion behaviour of the coated samples. In fact, it seems that the presence of the elements Ti, Ni and Al should play an important role as shown by the differences between the various N-containing coatings, despite their similar cross-section morphology. In order to try to understand the influence of these elements, we will first present a possible model to explain the pitting corrosion, which is in agreement with the SEM observations.

Taking into account the different forms of pits observed on the samples' surface for all types of film, which include:

- open pits at the centre of a circular ring consisting of corrosion products (Fig. 5a),
- very small bumps on the surface which already give rise to an EDXS signal of iron (Fig. 5c)
- small raised formations at the centre of a circular ring formed by corrosion products (Fig. 5e)

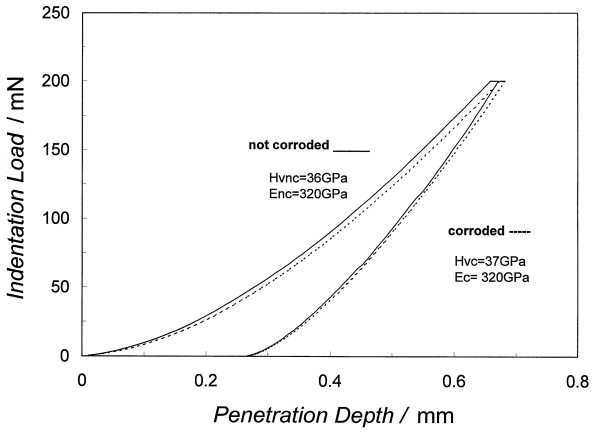

Fig. 7. Penetration depth versus indentation load curves obtained by the ultramicroindentation technique, for a W–Ti–N sputtered coating before and after corrosion.

it is probable that two different corrosion mechanisms take place individually or simultaneously. The first one is well known for pitting corrosion in chloride solution and begins by the penetration of ions through the coating (via microscopic defects) to the substrate. Oxidation of the substrate, which is much less inert than the film, then takes place. The accumulation of Fe^{3+} ions at that point could suck in chloride and OH^- ions to maintain electroneutrality. As soon as the first corrosion products are formed at the coating/substrate interface, significant stresses are developed leading to the opening of the pore which allows easier communication with the external solution (Fig. 9a and b). The presence of water leads to the formation of iron oxide hydrate species. The process then develops autocatalytically. The pressure increases and, when the amount of iron oxide is sufficient, a visible lifting of the film is observed, cracks possibly appear in the bubble until eventually it completely bursts (Fig. 9c and d).

Following the bursting of the bubble, the uncovered area of substrate suddenly increases, the concentrating of reagents at a specific point is not so favoured and so other corrosion mechanisms have also to be considered, as shown schematically in Fig. 10. The oxidation reaction continues to take place in the bottom of the pit whereas the reduction reaction, mainly oxygen reduction at these pH values (bulk solution pH ~ 5.5), should occur all over the coating surface, at a distance from the pit which is a function of the corrosion potential. The movement of Fe^{3+} and OH^- leads to the formation of iron oxide in the zone of solution in between these anodic and cathodic areas, and thence the characteristic circular ring observed by SEM. This can also occur simultaneously, but at a lower rate, with the corrosion of 'closed' pores presented above.

We now consider the way in which N, Ni, Ti and Al can influence the electrochemical results and corrosion mechanism of the coated samples. Their influence has to be attributed to their ability to restrict access of the different reagents to the sites of the corrosion reactions (ions, electrons, solution, ...) and to absorb the stresses generated by the formation of iron oxide in the pit under the film, hindering bubble bursting.

Concerning the first of these points, this can be divided into access of the solution and its components to the pit under the coating, and the other to the conduction of electrons through the substrate and coating to the sites of the reduction reactions. As mentioned above, films with N are denser, which makes access of the electrolyte solution to the interior of the pit more difficult. This can retard the autocatalytic development of the corrosion process.

Regarding the electronic conductivity different aspects have to be considered. Films containing N have higher resistivity than those without N, which is a possible contributing factor for their better corrosion behaviour [26,27]. Moreover, the deposition in a N reactive atmosphere can have also an indirect influence on coating resistivity. During the sputtering process there is some etching of the growing film, particularly when the deposition is done with the substrate negatively biased (as is the case in this work). Etching occurs preferentially for the lighter elements, i.e., Ni, Ti and Al. In the presence of nitrogen in the sputtering chamber, these elements are bonded to N at the surface of the growing film, which reduces their preferential etching and increases their percentage in the film. Thus, if the original target composition is the same, as here, the M (Ni, Ti and Al) content in the W–M–N films

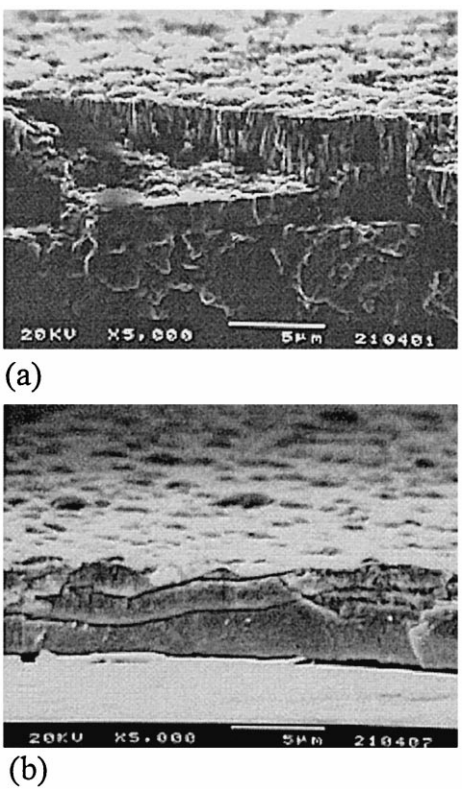

Fig. 8. SEM micrographs of the cross-section morphology of W–Ti–(N) sputtered coatings deposited without (a) and with (b) N_2 reactive gas.

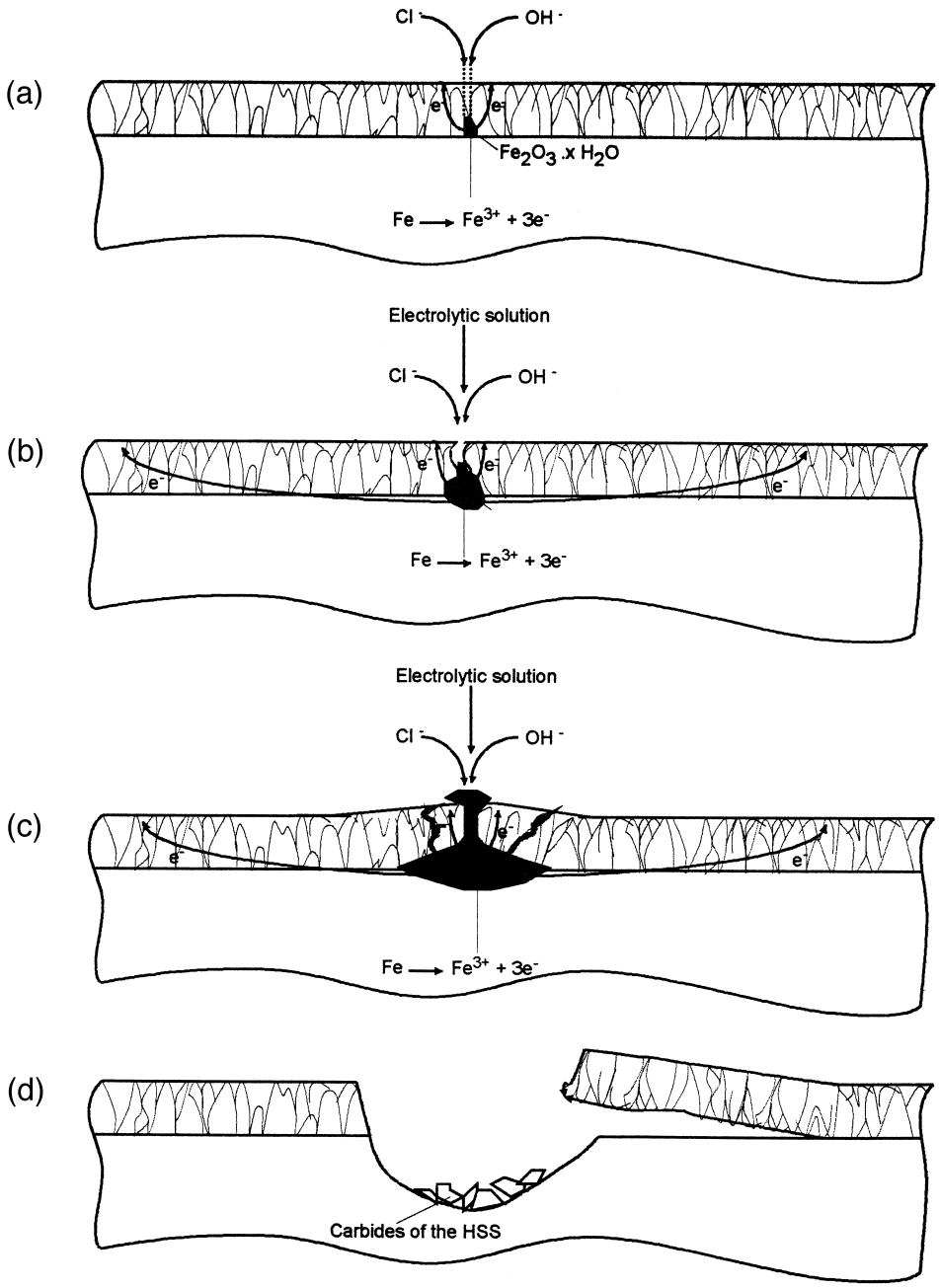

Fig. 9. Scheme of the corrosion process by pitting formation (a) → (d) of W–M–N sputtered coatings.

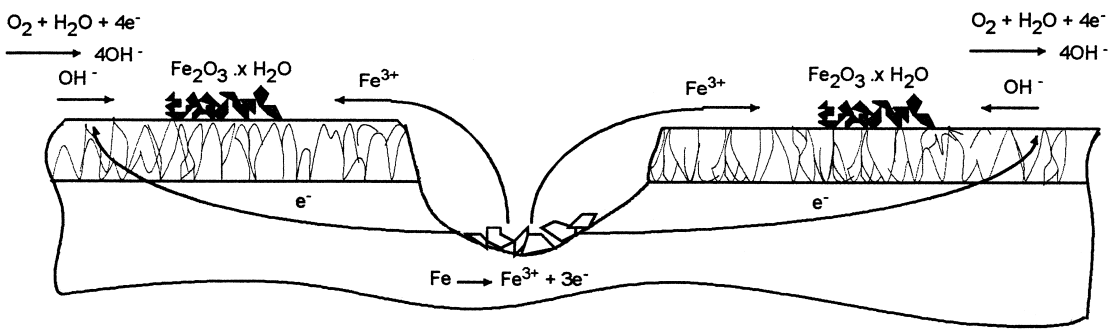

Fig. 10. Scheme of the formation of the circular ring of the corrosion products around the pits in the corrosion of W–M–N sputter-coated HSS M2 steel.

Table 6
Lc1 values determined by scratch-testing of the sputtered W–M–N films

Film	Lc1/N
W–Ni	40
W–Ni–N	23
W–Ti	30
W–Ti–N	51
W–Ti–Al	14
W–Ti–Al–N	68

is higher than in W–M films. So, if the M content is important for the corrosion resistance of W-based coatings, as will be explained below, the N content is also indirectly responsible for the observed variations.

It was discussed above that the simultaneous addition of Ni and N in sufficient amount to W-sputtered coatings produces amorphous structures, and so it is expected that W–Ni–N has a higher corrosion resistance than W–Ni. It is well known that the presence of Al in some alloys can give rise to the formation of a very thin continuous, passive layer (only some nanometers thick) and with very low electronic conductivity [19]. In the light of these observations, the corrosion behaviour of samples containing Al should be better than that of the other samples. It has also been shown that the addition of Ti to W–(N) coatings leads to increasing resistivity which can contribute to higher corrosion resistance [27].

The observed corrosion behaviour should also be related to the ability of the coatings to support the deformation imposed by the precipitation of the iron oxide inside the pit. The higher the coating ductility the more it can resist bubble bursting. The ductility of a material in the form of a thin coating is well characterized by scratch testing. In this test, the load corresponding to the first failure observed when a diamond stylus is dragged at increasing loads perpendicularly over a coated surface is called the critical load (Lc). Two types of critical loads can be defined, a cohesive value (Lc1), regarding the failure inside the coating itself, and an adhesive value (Lc2) related to the adhesion between the coating and the substrate. The Lc1 value gives, to a good approximation, the capacity of the coating to resist material deformation, i.e., its ductility. Table 6 gives the Lc1 values for these coatings. With the exception of W–Ni–(N), the coatings containing N have higher Lc1 values. Thus, for these coatings the bursting of the bubbles is retarded and some improvement in corrosion resistance should be expected.

The corrosion model developed in this section and shown in Fig. 9 is in agreement with electrochemical and non-electrochemical observations in this work and in previous studies by other research groups. It demonstrates the general similarities between the different types of coating and permits distinctions to be made between their corrosion resistances, according to the nitrogen and heavier element (Ti, Al, Ni) content.

4. Conclusions

A detailed study of the corrosion resistance of W–M–N (M = Ni, Ti, Al) coatings has shown that although corrosion proceeds at specific flaws in the coating in all cases, there is a beneficial influence of N and some differences according to the identity of M. Coatings containing Al present better corrosion behaviour than the other coatings. Electrochemical observations supported by scanning electron microscopy, X-ray diffraction and microindentation have led to the elaboration of a general model for the localised corrosion process. This involves as first step the penetration of electrolyte through sub-microscopic flaws in the coatings followed eventually by film rupture and pitting corrosion.

The general implications for the use of sputter-coated thin films are, given that sub-microscopic porosity is probably unavoidable, that the incorporation of nitrogen in these types of film to alter the structure, apart from making the films amorphous, is a very useful way to mitigate the effects of corrosion in aggressive aqueous environments.

Acknowledgements

Financial support from Junta Nacional de Investigação Científica e Tecnológica (JNICT), Portugal, project PBIC/C/CTM/1383/92 is gratefully acknowledged.

References

[1] S. Berg, N. Eguchi, V. Grajewski, S.W. Kim, E. Fromm, Surf. Coat. Technol. 49 (1991) 336.
[2] I. Montero, C. Jimènez, J. Perrière, Surf. Sci. 251/252 (1991) 1038.
[3] R. Brown, M.N. Alias, R. Fontana, Surf. Coat. Technol. 62 (1993) 467.
[4] M. Ürgen, A.F. Çakir, O.L. Eryilmaz, Berichtsband EAST Kongr., 1993, p. 26.
[5] H. Barànková, L. Bárdos, S. Berg, J. Electrochem. Soc. 141 (1994) L8.
[6] S.D. Chyou, H.C. Shih, T.T. Chen, Corros. Sci. 35 (1993) 337.
[7] K. Hashimoto, N. Kumagai, H. Yoshioka, J.H. Kim, E. Akiyama, H. Habazaki, S. Mrowec, A. Kawashima, K. Asami, Corros. Sci. 35 (1993) 363, and references therein.
[8] A. Cavaleiro, M.T. Vieira, G. Lemperiere, Thin Solid Films 185 (1990) 199.
[9] A. Cavaleiro, M.T. Vieira, G. Lemperiere, Thin Solid Films 197 (1991) 237.
[10] A. Cavaleiro, M.T. Vieira, Mater. Sci. Eng. A140 (1991) 631.
[11] A. Cavaleiro, M.T. Vieira, G. Lemperiere, Thin Solid Films 213 (1992) 6.
[12] A. Cavaleiro, M.T. Vieira, G. Lemperiere, Thin Solid Films 228 (1993) 80.
[13] C. Ringas, F.P.A. Robinson, S.B. Luyckx, J.P.F. Sellschop, Surf. Eng. 6 (1990) 194.
[14] C. Louro, A. Cavaleiro, Surf. Coat. Technol. 74/75 (1995) 998.
[15] C. Louro, A. Cavaleiro, J. Electrochem. Soc. 144 (1997) 259.
[16] C.M.A. Brett, A. Cavaleiro, Mater. Sci. Forum 192–4 (1995) 797.
[17] C.M.A. Brett, C.-M. Nimigean, Thin Solid Films 311 (1997) 1.

[18] H. Yoshioka, Q. Yan, K. Asami, K. Hashimoto, Mater. Sci. Eng. A134 (1991) 1054.
[19] H.J. Wondergem, A. Heger, J.J. van der Broek, Thin Solid Films 249 (1994) 6.
[20] A.C. Trindade, A. Cavaleiro, V. Fernandes, J. Testing Eval. 22 (1994) 365.
[21] C.M.A. Brett, P.I.C. Melo, J. Appl. Electrochem. 27 (1997) 959.
[22] B. Trindade, M.T. Vieira, E. Bauer-Grosse, Thin Solid Films 252 (1994) 82.
[23] Joint Committee on Powder Diffraction Standards, Powder Diffraction File, International Centre for Diffraction Data, Swarthmore, PA, Card 8-98.
[24] A. Cavaleiro, C. Louro, V. Fernandes, C.M.A. Brett, Vacuum, in press.
[25] A.G. Dirks, R.A.M. Wolters, A.E.M. De Veirman, Thin Solid Films 208 (1992) 181.
[26] K. Affolter, H. Kattelus, M.-A. Nicolet, Proc. Mater. Res. Soc. Symp. 17 (1985) 167.
[27] H. Ramarotafika, G. Lemperiere, Thin Solid Films 266 (1995) 267.